sciendo

Transport and Telecommunication, 2024, volume 25, no. 1, 77–96
Transport and Telecommunication Institute, Lomonosova 1, Riga, LV-1019, Latvia
DOI 10.2478/ttj-2024-0008

COMPUTATIONAL FLUID DYNAMICS ANALYSIS OF FLOW CHARACTERISTICS AND HEAT TRANSFER VARIABILITIES IN MULTIPLE TURBINE BLADE COOLING CHANNELS

Adham Ahmed Awad Elsayed Elmenshawy[1], Iyad Alomar[2], Ali Arshad[3], Aleksandrs Medvedevs[4]

[1,3]Riga Technical University
Kīpsalas 6a, Riga, LV-10148, Latvia
[1]Adham-Ahmed-Awad-Elsayed.Elmenshawy@rtu.lv, [3]Ali.Arshad@rtu.lv
[2,4]Transport and Telecommunication institute
Lomonosova 1, Riga, LV-1019, Latvia
[2]Alomar.I@tsi.lv, [4]Medvedevs.A@tsi.lv

In the realm of gas turbine engine technology, turbine blades are persistently subjected to extreme thermal conditions due to prolonged exposure to high-temperature gases. Given this operating environment, devising effective cooling strategies is paramount for ensuring the turbine's safety and longevity. Despite the critical nature of this issue, existing literature scarcely addresses cooling channels that incorporate factors like variable cross-sectional attributes and rotational effects. In this study, Computational Fluid Dynamics (CFD) and numerical methodologies were employed to analyze the flow mechanism and performance of three distinct cooling channels characterized by variable cross-sectional features. The results indicate a marginal thermal performance improvement of up to 3% for U-shaped cooling channels, specifically at a Reynolds number of 20,000, in comparison to Net cooling channels. Conversely, jet impingement channels outperform U-shaped channels by an impressive margin of over 11%. Additionally, at a Reynolds number of 60,000, jet impingement cooling channels manifest a significant upsurge of nearly 25% in the ratio between average Nusselt number, and the reference Nusselt number when compared with U-shaped and Net cooling channels.

Keywords: Conjugate heat transfer, thermal performance, turbine, blade cooling channels

1. Introduction

Gas turbine blades have endured prolonged exposure to abrasive high-temperature gases in challenging environments. Presently, advanced gas turbines operate with inlet gas temperatures exceeding 1600 degrees Celsius, surpassing the material's permissible limits (Xu *et al.*, 2023). The future advancement of gas turbines will inevitably involve even higher gas temperatures. Therefore, the research and development of cutting-edge and efficient cooling technologies for turbine blades hold significant importance. These innovations aim to safeguard gas turbine blades and subsequently reduce maintenance expenses. In recent years, researchers have shown a strong interest in dimple and protrusion structures due to their efficiency and low resistance characteristics. (Afanasyev *et al.*, 1993) conducted a study on the turbulent friction and thermal transmission properties of channels featuring dimples. (Chyu, 1997) conducted experiments to explore the impact of Reynolds number on channels with teardrop-shaped and spherical dimples. (Moon *et al.*, 2000) examined enhanced heat exchange and resistance performance in channels featuring a single-sided socket structure. (Burgess, et al., 2003) investigated the effects of Nusselt number and dimple depth on channel behavior delved into the comprehensive performance of channels with dimple configurations and V-shaped ribs. (Shen *et al.*, 2013) focused their research on the influence of suction holes and dimple structures on the flow characteristics within a U-shaped channel.

Blade malfunctions stemming from cooling inadequacies can severely compromise both the efficiency and dependability of gas turbine engines (Nozhnitsky, 2018). Elevating the inlet gas temperature can maximize the energy harnessed from combustion, thereby boosting the engine's efficiency. However, this temperature increase also subjects the turbine blades to heightened stress, impacting their resilience and longevity (Yamane *et al.*, 2012). Consequently, there is an industry-wide push to use materials with superior heat tolerance and cutting-edge cooling solutions to maintain the blades under secure operational conditions.

The challenge is to find the ideal equilibrium between enhanced operating temperatures and secure functionality (Ackert, 2011). Cooling-related issues can emanate from various factors, including obstructed cooling channels, suboptimal flow rates, or unsatisfactory coolant temperatures. These can culminate in the blades overheating, which may lead to their failure. A compromised blade can, in turn, inflict damage on additional engine parts, distort airflow, and induce imbalanced rotations potentially resulting in catastrophic engine failure (Elmenshawy and Alomar, 2022). To counter these issues, meticulous cooling system design and maintenance are indispensable. Sophisticated cooling setups, computational optimization techniques, and Conjugate Heat Transfer (CHT) analyses are increasingly being deployed to tackle the complexities induced by rising turbine inlet temperatures. Such advanced cooling systems aim for a nuanced balance adequate blade cooling without performance-efficiency trade-offs (Coletti *et al.*, 2012). Optimization algorithms guide the search for the most effective cooling strategies, supported by numerical simulations (Nirmalan and Hylton, 1989). CHT analyses contribute to a deeper understanding of intra-blade heat transfer, thereby informing improvements in cooling configurations. By synergizing these multiple approaches, professionals in the gas turbine sector are better equipped to design cooling mechanisms that proficiently manage elevated temperatures while preserving engine safety and reliability. While existing literature abounds with research focusing on the architecture of blade cooling channels, there is a noticeable gap in studies that concurrently examine turning vanes, variable cross-sectional attributes. This study addresses this gap by selecting a cooling channel with varying different cross-sections as its baseline model. Sourced from an actual gas turbine blade, this model incorporates protrusion structures on its surface. The investigation includes a comprehensive analysis of flow dynamics, heat transfer, and resistance features for channels equipped with different designs of cooling channels. In the scope of this research, we employed ANSYS FLUENT for Computational Fluid Dynamics (CFD) solving, while mesh creation was facilitated through ANSYS ICEM-CFD. The latter was specifically chosen for its capability to produce high caliber meshes compatible with CFD analyses. Collectively, these software tools enabled us to execute in-depth and precise CFD simulations focused on the cooling setups within a gas turbine blade. MATLAB code used for numerical analysis with experiment data and simulation results.

2. Methodology

The core objective of the present study is to engineer a state-of-the-art design for cooling channels in turbines, targeting a considerable augmentation in thermal efficiency and cooling efficacy, coupled with a reduction in drag forces. Utilizing cutting-edge Computational Fluid Dynamics (CFD) models and empirical analyses, the study aspires to establish a channel configuration that is versatile across an extensive range of Reynolds numbers and diverse flow regimes. A key focus of this investigation lies in an exhaustive examination of the fluid dynamics at various critical segments within the cooling channels, such as bends and junctions, with the intent to pinpoint zones requiring optimization. MATLAB algorithms will be deployed for data processing, allowing for rigorous computational analysis and comparative evaluation based on experimental findings.

2.1. U-bend optimization (Case 1)

The main concept of this design is to cover more area in the trailing edge. A diameter of 6.3 mm from the original NASA C3X cooling channel was adopted as in Helton, as suggested by Hylton a modified 20 mm U-bend from the original channel with a bend angle 129.5°, and symmetry were also applied for the full entire length of 76.2 mm, as shown in Figure 1. In this case the main advantage to increase the angle in U bend, so as to help minimize pressure drop and the drag. The geometrical turbine cooling channel design was created using ANSYS Workbench.

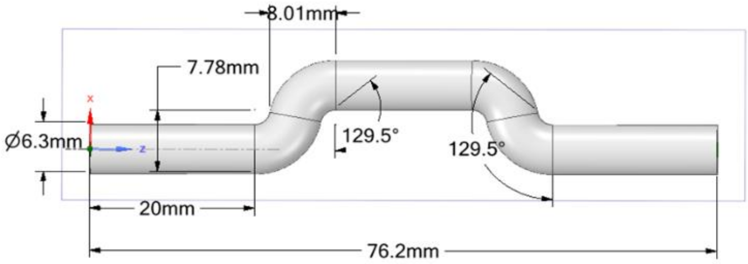

Figure 1. U-bend model configuration

The author installed the cooling channel geometry and computational domain for starting meshing for this case, Figure 2 presents the geometry before meshing and shows the computational boundaries selected for this U bend geometry.

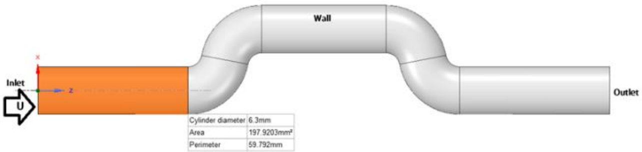

*Figure 2***.** 3D U-bend model flow domain

The size and properties of a smooth pipe with known experimental data were chosen to analyze the hydrodynamic and heat transfer characteristics through a straight pipe. The size and features of the smooth pipe from the experimental investigation were employed in this study (Al-Obaidi and Chaer, 2021). The creation of the channel design used three-dimensional unstructured meshing.

Mesh carried out for this model, with bounding length (14.44, 6.3, 76.2) mm, total volume 2589 mm^2. One bode selected for this case. Mesh Created used CFD, Using CFX Solver. Element size 0.2 mm for this case, this provides more accuracy for the flow conditions.

Since transport phenomena for momentum and other scalar quantities are most prominent in regions close to the wall, where solution variable gradients are larger. In this analysis, the inner layer is divided into three zones, each characterized by its respective non-dimensional distance, known as the wall Y+ value. This value is analogous to the local Reynolds number. Specifically, the viscous sub-layer corresponds to Y+ values below 5, the buffer or transitional layer ranges from 5 to 30, and the fully turbulent layer falls between 30 and 60. For the purposes of this study, we assumed a viscous sub-layer by selecting a Y+ value of 1. Air serves as the fluid medium for this investigation, with a density of 1.229 kg/m^2 and a viscosity of 0.0000173. The normal wall distance, denoted as Y, was calculated using a specific formula:

$$Y = \frac{Y^+ \nu}{u_\tau}, \tag{1}$$

where ν is the fluid viscosity, and u_τ is fraction velocity which can be calculated with:

$$u_\tau = \sqrt{\frac{\tau_w}{\rho}} \ , \tag{2}$$

where τ_w is the wall shear stress which can be calculated with:

$$\tau_w = 0.5 \ C_f \rho \ u^2, \tag{3}$$

where C_f is Skin fraction coefficient.

$$C_f = \frac{0.058}{R_e^{0.2}}, \tag{4}$$

where R_e is Reynolds number.

The author used equations above to calculate the normal distance to wall which is 0.00213 mm. Mesh inflation is done with using normal distance to wall as the first layer thickness, with maximum layers 10, and growth rate 1.35. Mesh contained 3962979 node and 969878 element, Figure 3 presents the mesh configuration, and Figure 4 presents the inflation layers.

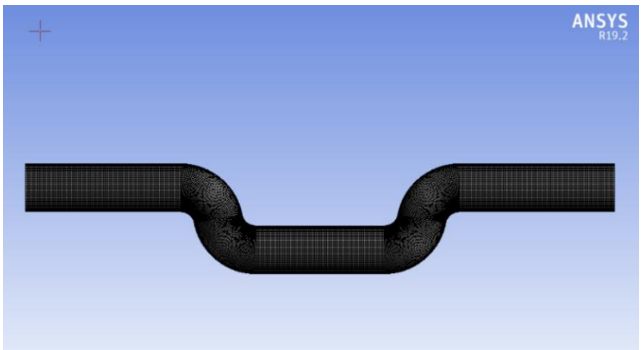

*Figure 3***.** 3D U-bend mesh configuration

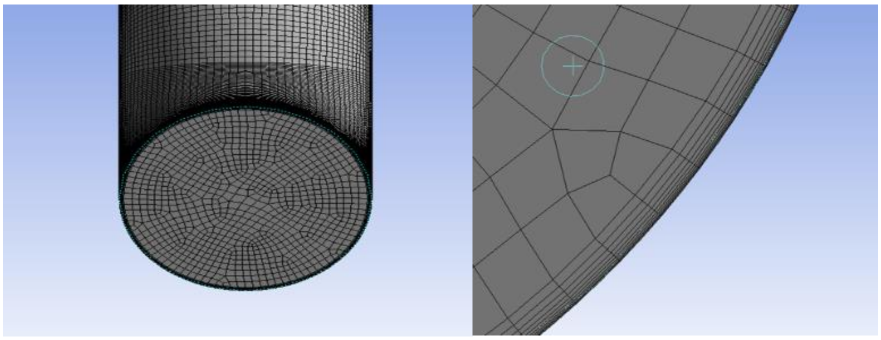

Figure 4. 3D U-bend Inflation layers

The aspect ratio of mesh elements emerges as a critical variable in the pursuit of reliable and efficient CFD analyses. Its influence extends to the credibility and precision of the simulation's numerical outcomes. Hence, meticulous attention to this aspect ratio is indispensable, more so in specialized applications such as the cooling channels in turbines where exactitude is paramount. In this context, Figure 5 delineates the quality of the mesh through its aspect ratio, providing empirical evidence written for its pivotal role in the computational study.

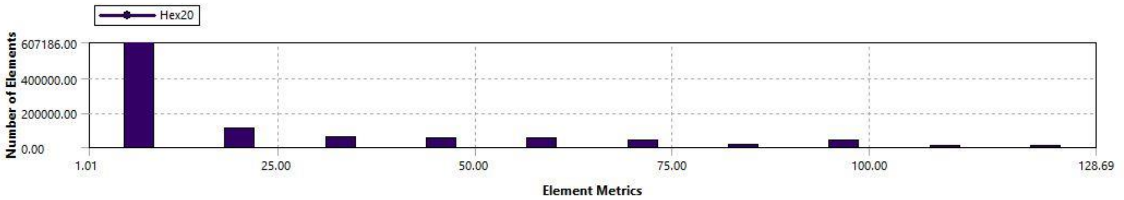

Figure 5. U-bend mesh quality metrics

2.2. Net bend cooling channels design (Case 2)

The core design principle aims to broaden the cooling coverage around the trailing edge of the turbine blade. Utilizing the original NASA C3X cooling hole diameter of 6.3 mm, as referenced from Helton's research, the design features three net channels strategically positioned between every two existing channels. The design also integrates symmetry and has an overall length of 76.2 mm. Within this framework, two Net channels each have a width of 0.52 cm, while the middle channel is slightly narrower at 0.42 cm, as illustrated in Figure 6. The key advantage of this layout is the enhanced surface area available for cooling. To bring this design concept to fruition, computational modeling was performed using ANSYS Workbench.

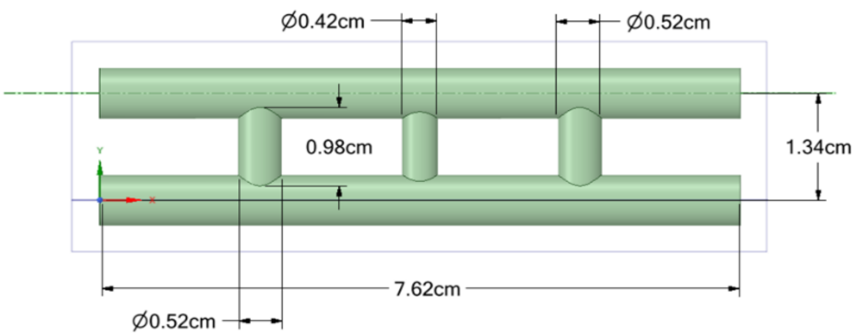

Figure 6. Net bend optimized model

The size and properties of a smooth channel with known reference experimental data were chosen to analyze the fluid dynamics and heat transfer characteristics through a straight channel. The size and features of the smooth channel were obtained from the previous studies (Al-Obaidi and Chaer, 2021).

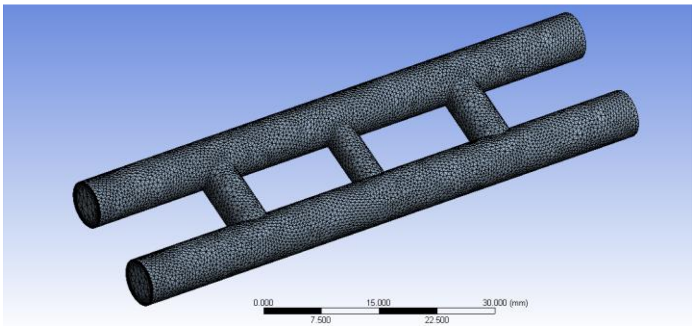

Figure 7. Net channels mesh configuration

The creation of the channel design used three-dimensional unstructured meshing. Mesh carried out for this model, with bounding length (14.44, 6.3, 76.2) mm, total volume 2589 mm^2. One bode selected for this case. Mesh Created used CFD, Using CFX Solver. Element size 0.5 mm for this case, this to provide more accuracy for the flow conditions. The author used equations above to calculate the normal distance to wall which is 0.00213 mm. Mesh inflation has been performed with using normal distance to wall as the first layer thickness, with 10 layers, and growth rate 1.2. Mesh contained 116291 node, and 264386 element, Figure 7 presents the mesh configuration, and figure 8 shows the inflation mesh layers.

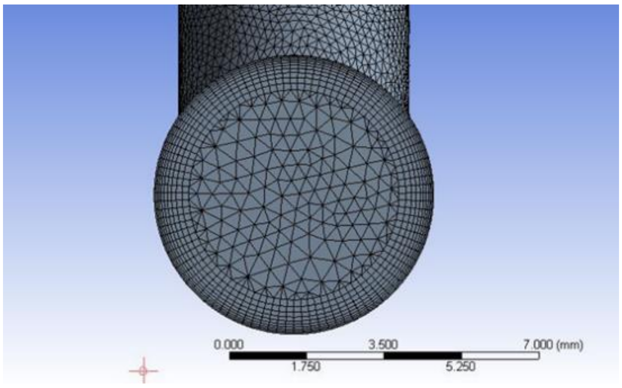

Figure 8. Inflation mesh layers

The mesh element's aspect ratio is a key factor in achieving accurate and trustworthy CFD simulations. Its role is crucial in determining the validity and exactness of the numerical results generated by the simulation. This is especially critical in specialized use-cases like turbine cooling channels, where high precision is essential. Figure 9 offers a detailed evaluation of the mesh quality via its aspect ratio, underscoring its significant impact on the overall reliability of the computational analysis.

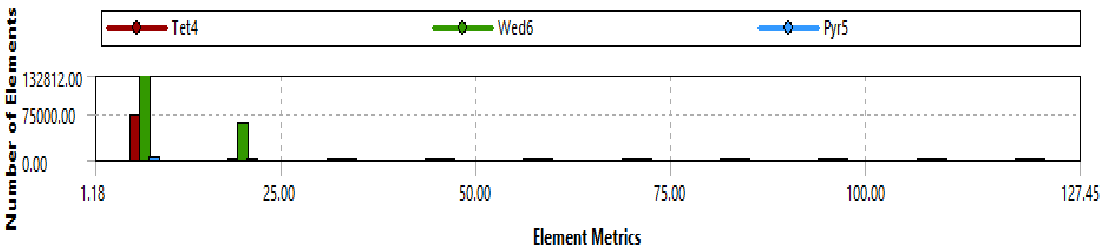

Figure 9. Mesh aspect ratio quality for net channels

2.3. Jet impingement cooling channels optimization (Case 3)

In the current study, the focus was on enhancing the cooling effectiveness of gas turbine components through an optimized jet impingement setup. The study yielded promising outcomes, specifically an improved heat transfer coefficient and a reduced blade leading edge temperature, without causing a notable increase in pressure drop. This underscores the significance of precisely selecting jet impingement variables in cooling system designs for gas turbine elements. By retaining the mesh structure from the foundational model and incorporating insights from Glynn's research (Glynn *et al.*, 2005), it was confirmed that reducing the diameter of the jet nozzle can significantly enhance heat transfer. Additionally, this study adheres to Yamane's guidelines on optimal nozzle height-to-diameter (H/DJ) ratios, which should range between 2 and 8. For this study, a jet diameter of 1.94 mm was selected, yielding an H/DJ ratio of 8, aligning well with Yamane's suggested parameters. Furthermore, the jet spacing to jet diameter (S/DJ) ratio was maintained between 4 and 8, with a selected jet spacing of 11.44 mm, resulting in an S/DJ ratio of 5.89. so Utilizing the ANSYS Workbench, the pipe's geometrical design was created, this optimized design carried out to be three jet channels (Yamane *et al.*, 2012). Figure 10 and Figure 11 present Jet impingement type cooling channels configuration.

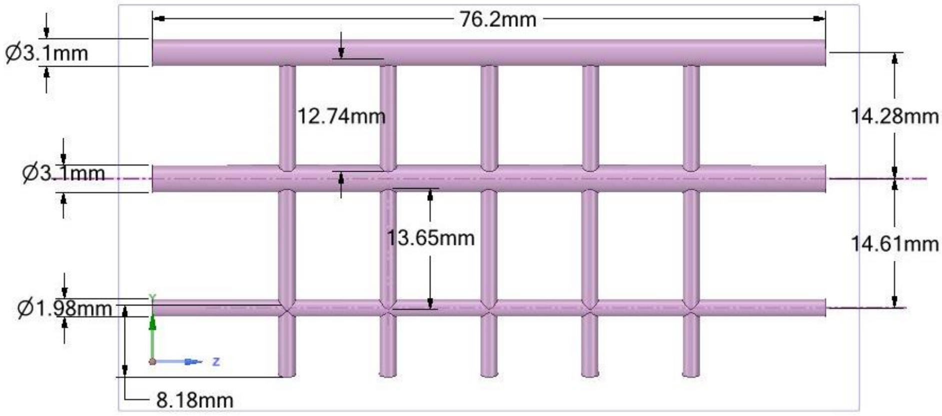

Figure 10. Jet impingement cooling channels configuration

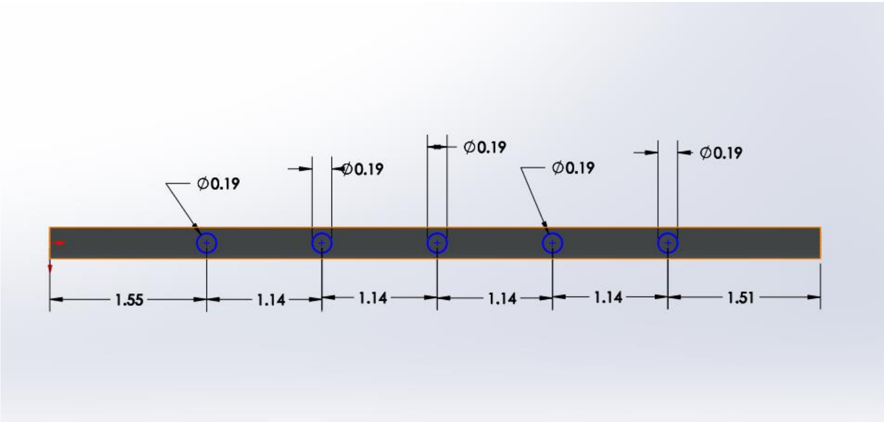

Figure 11. Jet impingement optimized cooling channels configuration

For the computational model in this study, the mesh was designed using CFX Solver. The mesh dimensions were set at (16.045 mm, 38.256 mm, 76.2 mm) with a total volume of 1871.9 mm^2, containing 243,212 nodes and 664,928 elements. A single domain was chosen for the analysis, and the element size was set at 4.338 mm to enhance flow condition accuracy. Figure 12 presents Jet impingement mesh configuration.

Regarding the dynamics of scalar and momentum transports, these are particularly active in regions close to the wall, where solution variable gradients are high. The mesh in these areas was divided into three distinct zones, each identified by its respective Y+ value, a non-dimensional distance parameter related to the local Reynolds number. In this study, the Y+ values were categorized as follows: less than 5 for the viscous sub-layer, between 5 and 30 for the buffer or transition zone, and 30 to 60 for the fully turbulent flow zone. For this analysis, a Y+ value of 1 was selected, corresponding to the viscous sub-layer. The fluid medium was air, having a density of 1.229 kg/m^2 and a viscosity of 0.0000173. Based on these parameters, the normal wall distance 'Y' was computed using a specific Equation 1.

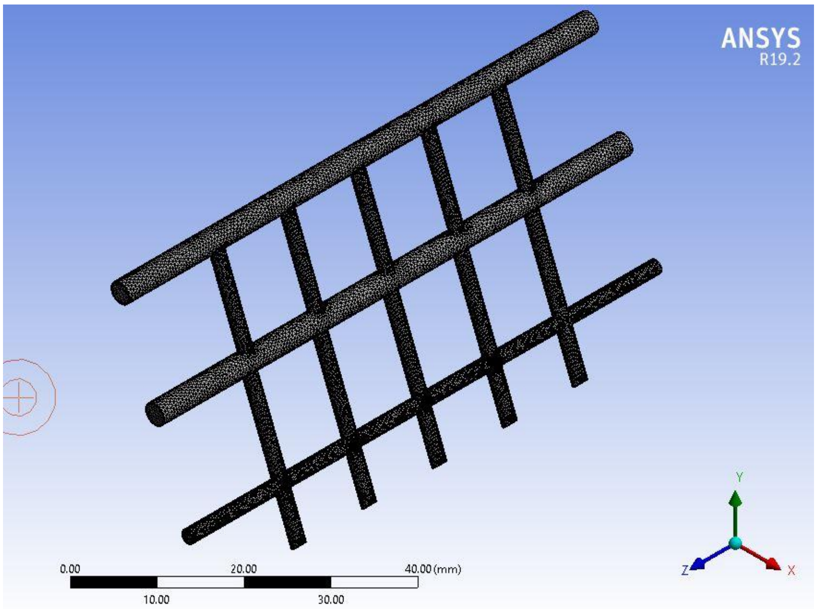

Figure 12. Jet impingement mesh configuration

The aspect ratio of the mesh elements is an essential component for ensuring the reliability and accuracy of CFD simulations. Its significance cannot be overstated, particularly in specialized applications like turbine cooling channels, where precision is crucial. Figure 13 presents an examination of the mesh aspect ratio, thereby highlighting its critical role in contributing to the integrity and accuracy of computational research. In Figure 13, the aspect ratio chart of the grid schemes reveals the good quality of the mesh.

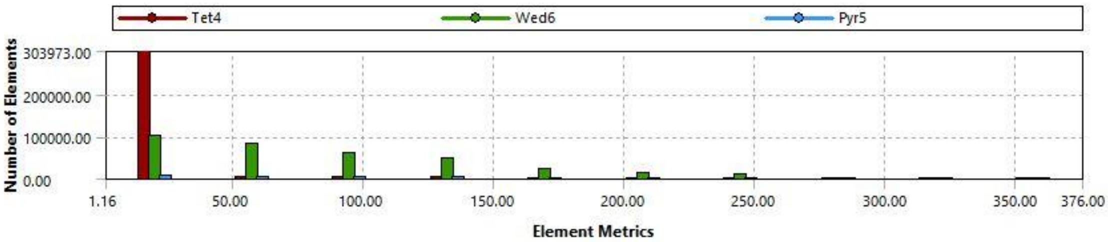

Figure 13. Jet impingement mesh aspect ratio quality

2.4. Numerical method

The dynamics of fluid flow and heat transfer adhere to specific physical principles, and the governing equations serve as mathematical representations of these fundamental laws. These equations are typically solved using numerical methods to investigate the underlying dynamics within fluid flow and heat transfer phenomena. This exploration yields valuable theoretical insights that can guide practical engineering applications. The solved equations encompass the mass equation, momentum equation, and energy equation, with the addition of the fluid state equation to ensure a comprehensive solution.

$$\frac{\partial \rho u_i}{\partial x_i} = 0, \tag{5}$$

$$\frac{\partial \rho u_i u_j}{\partial x_i} = \rho g_i + F_i - \frac{\partial P}{\partial x_i} + \frac{\partial}{\partial x_i} \cdot \left(2\mu S_{ij}\right), \tag{6}$$

$$\frac{\partial \rho u_i E_0}{\partial x_i} = \rho u_i F_i - \frac{\partial q_i}{\partial x_i} + \frac{\partial}{\partial x_j} \cdot \left(u_j T_{ij}\right), \tag{7}$$

$$\rho = f(\rho, T), \tag{8}$$

where F_i represents the body force, P stands for pressure, S_{ij} denotes the strain rate tensor, E_0 signifies the total internal energy, and T_{ij} corresponds to the surface force.

In the current investigation, we implement the Reynolds-Averaged Navier-Stokes (RANS) approach, using widely used finite-volume solver for our computations. Previous research involving a three-pass channel structure equipped with turning vanes and ribs was explored by Guo *et al*. in 2021. According to their studies, the Shear-Stress Transport (SST) k-ω turbulence model demonstrated a maximum deviation of 6.5% from the experimental data. This was notably lower than the discrepancies found with Realizable k-ω and RNG k-ω models, which showed errors of 19.3% and 22.4% respectively. Therefore, our study opts to employ the SST k-ω model for more rigorous analysis.

For the evaluation of pressure drops, this research utilizes Equation 10, which derives from the Darcy-Weisbach equation, cited from Brown's work in 2002 (Brown, 2002). The formula presumes the flow to be fully developed, in turbulent motion, and incompressible, with negligible variations in elevation or velocity along the conduit's length.

$$\Delta P = f\frac{L}{D}\frac{\rho U^2}{2g}, \tag{10}$$

where ΔP is the pressure drop, f is the friction factor, L is length of the channel or pipe, D is the diameter of the channel, ρ is the density, U is the mean velocity of the fluid, and g is the gravitational acceleration.

2.5. Parameter definition

In the experimental setup by Wang, the central vane of the C3X transonic turbine received cooling via air circulation from the hub towards the deck through a series of ten cylindrical channels. The blade was constructed from ASTM Type 310 stainless steel. Wang's model replicated these conditions, defining the material properties of ASTM 310 stainless steel to include a specific heat capacity (Cp) of 502 J/(kg·K) and a density (ρ) of 8030 kg/m³ (Wang *et al*., 2014; Wang *et al*., 2015).

The Reynolds Number, denoted as (ReD), and hydraulic diameter (D_C) for each cooling channel were derived from key parameters including fluid mass flow rate ($\dot{m}$), viscosity (μ), and coolant density (ρ). These calculations were undertaken to ensure outlet pressure compatibility with NASA's C3X data, by matching the inlet Reynolds Number from 10000 to 50000.

Reynolds Number serves as a pivotal criterion for understanding flow behavior in each cooling channel. Turbulent flows, generally marked by higher Reynolds Numbers, tend to favor elevated heat transfer rates but also lead to transitional flow regimes. These transitional phases present computational challenges, making it difficult to precisely model both flow behavior and heat transfer characteristics within the cooling system.

For the hydraulic diameter-based Reynolds Number (ReD), Equation 11 was employed to characterize each cooling passage, using (D_C) as the foundational metric for calculation. This approach aids in capturing the nuances of flow dynamics, which is crucial for accurate simulation and thermal performance evaluation.

$$R_{eD} = \frac{\frac{\dot{m}}{A}Dc}{\mu}. \tag{11}$$

The Nusselt number is a dimensionless number used in heat transfer calculations ant it’s important to measure of the convective heat transfer relative to conductive heat transfer across a boundary which was obtained by:

$$N_u = \frac{qD_C}{(T_w - T_f)\lambda}, \tag{12}$$

where T_w represents the wall temperature, T_f stands for the average inlet temperature based on mass flow, and λ denotes the thermal conductivity of the fluid. The variable q represents the heat flux.

The reference Nusselt Number (N_{u0}) equation was used to determine the HTC of each cooling channel (Yang *et al*., 2017).

$$N_{u0} = \left(0.023 p_r^{0.5} R_e^{0,8}\right). \tag{13}$$

Resistance factor f is represented as follow:

$$f = \frac{\Delta p D_C}{2\rho L u_{in}^2}, \quad (14)$$

where L is the flow Length, and Δp is the pressure drop.

The reference resistance factor f_0 (Wang *et al.*, 2018):

$$f_0 = 0.507 R_e^{-0.3}. \quad (15)$$

TP, standing for comprehensive thermal performance, provides a comprehensive assessment of the cooling channel characteristics and can be computed as follows:

$$T_P = \left(\frac{N_{u_a}}{N_{u0}}\right) \times \left(\frac{f}{f_0}\right)^{-1/3}, \quad (16)$$

where N_{ua} is the average Nusselt number of all heating surface including PS, SS, and tip wall surface.

Drag force calculated by Eq. (17)

$$F_d = f \times \frac{\mathrm{L} \times \rho \times U^2}{D_C} \times A, \quad (17)$$

where *L* is the length, fluid density *ρ*, fluid velocity *U*, and hydraulic diameter is *Dc*.

2.6. Boundary condition

The boundary conditions for the analysis were taken from the experimental test code 4311, run 148 (Hylton and York, 1983), Heat flux to the wall is 1135 Watt/m^2/K. The constant mass flow rate for inlet is calculated by Reynolds Number, the inlet channel temperature of the cooling fluid is 298.15K. Table 1 presents the boundary condition which the authors used for simulation. The outlet pressure used for this study is 1 atm. For simplicity, air as ideal gas was used as the cooling fluid in the channels. Table 1 presents full details for the boundary condition for this study.

Table 1. Initial flow condition for the domain

P_0	Heat flux to the wall	M_i	l	T_u	T_w/T_g	M_e (x = 0.09836)
321KPa	1135 Watt/m^2/K	0.17	0.016m	6.5%	0.73	0.9

3. Results

3.1. Cooling effect and performance

The present research undertakes a comprehensive comparison of diverse cooling channel configurations, employing Computational Fluid Dynamics (CFD) simulations complemented by calculations executed in MATLAB. The comparative analysis is structured into three distinct segments, each homing in on specialized cooling configurations and their respective characteristics. Data generated from the study, such as temperature and pressure contour plots, are critically evaluated. This multi-faceted comparison aims to unearth the optimal cooling arrangement by examining key metrics, including Nusselt numbers, fraction factors, thermal performance, and drag force, particularly in critical zones within the cooling channels. This analytical approach aims to not only identify the most efficient cooling configuration but also offer insights into potential avenues for performance enhancement.

3.1.1. Performance analysis for U-bend cooling channel

Figure 14 illustrates the results of a Computational Fluid Dynamics (CFD) simulation, providing insights into the temperature distribution within U-bend channels. Notably, the simulation reveals that the maximum temperature within these channels during fluid flow reaches approximately 529 Kelvin within these channels during fluid flow.

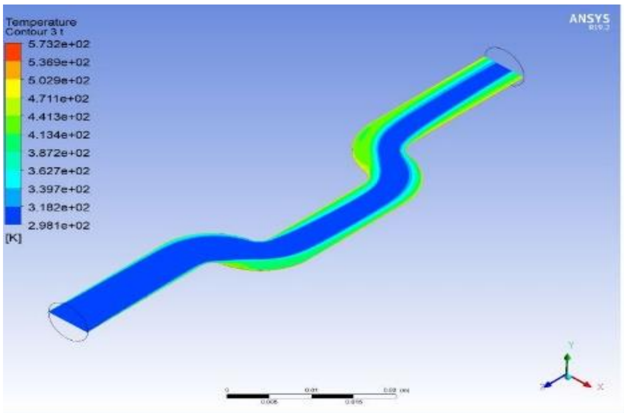

Figure 14. U-bend temperature counters

Figure 15 presents velocity contour plots, which vividly depict an intriguing phenomenon: a noticeable increase in velocity around the corners of the bend, with the maximum velocity recorded at an impressive 156 meters per second (m/s).

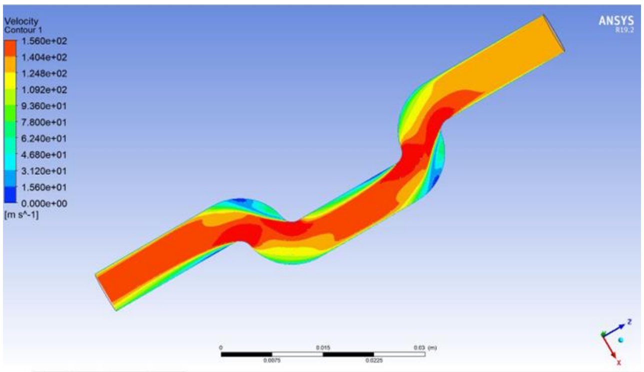

Figure 15. U-bend velocity counters

Figure 16 presents U-bend cooling channels pressure counters plots that offer valuable insights into the system's dynamics. These contours reveal an interesting observation: pressure levels begin to elevate notably at the corners of the bend, which have been designed with an angle of 129 degrees. The maximum pressure recorded within the system reaches an impressive 15,130 Pascals (Pa). Furthermore, as the channels progress towards their termination, the author discovered a substantial pressure drop, with the pressure eventually decreasing to 3,076 Pa. This information highlights the impact of channel design on pressure distribution throughout the system.

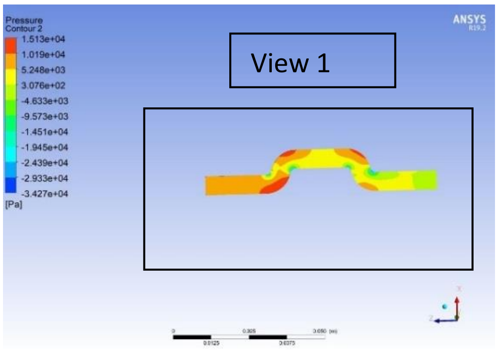

Figure 16. U-bend pressure counters

Figure 17 illustrates the relationship between the friction factor and Reynolds number, particularly at the bends within the cooling channels. Four most critical locations within the U-bend cooling channel were selected, i.e., location A, B, C and D. These are the locations where the flow experiences resistance due to the geometric configuration of bends, therefore, these locations are important where the drag force may have the greatest impact due to pressure drop. Notably, the fraction factor peaks at 0.92 at position A when the Reynolds number is 10,000. As the Reynolds number escalates to 50,000, there is a discernible attenuation in the fraction factor. This suggests a significant influence of Reynolds number on the fraction factor, especially at critical points such as channel turns.

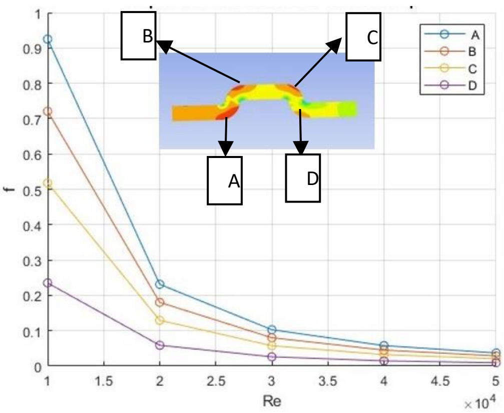

Figure 17. Graph between fraction factor (f), and (Re) Reynolds Number for U-channel

As seen in figure 18 from the calculated values, the maximum drag force is at location A which is the first bend in the cooling channel. On the positive side, the flow pressure is sufficient to travel across the channel with carried momentum energy to perform the cooling process, as observed in velocity contours of Figure 15. Intriguingly, this level of drag force maintains its constancy across a Reynolds number range spanning from 10,000 to 50,000. From the simulated results of CFD analysis and the MATLAB code, it can be concluded that the U-bend channel design offers good cooling, but the drag force is slightly higher.

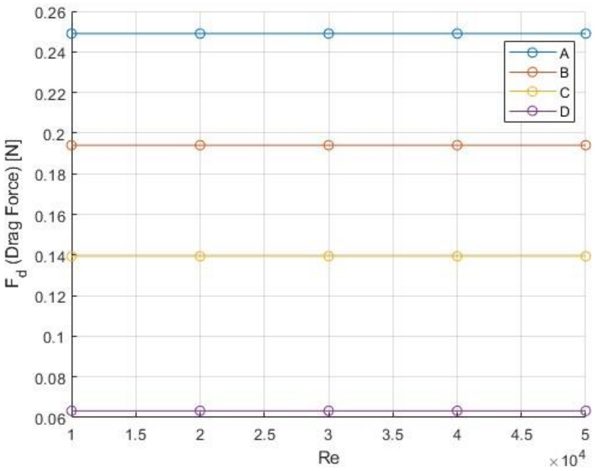

Figure 18. Graph between drag force, and Reynolds Number for U-channel

Elucidates the relationship between drag force and Reynolds number, highlighting a noteworthy observation: the maximum drag force plateaus at 0.25 N. Intriguingly, this level of drag force maintains its constancy across a Reynolds number range spanning from 10,000 to 50,000. This constancy in drag force over a broad Reynolds number spectrum suggests a level of invariance that may have implications for fluid flow dynamics, especially in regimes characterized by these Reynolds numbers.

3.1.2. Investigation performance for Net bend cooling channels design

Figure 19 presents the outcomes of a Computational Fluid Dynamics (CFD) analysis aimed at understanding thermal behavior within the network of channels. The data explicitly highlights those peak thermal values within the channels plateau at around 541 K during the fluidic flow. This peak temperature point may have significant implications for the material properties and operational conditions, emphasizing the importance of thermal management strategies within these networked systems.

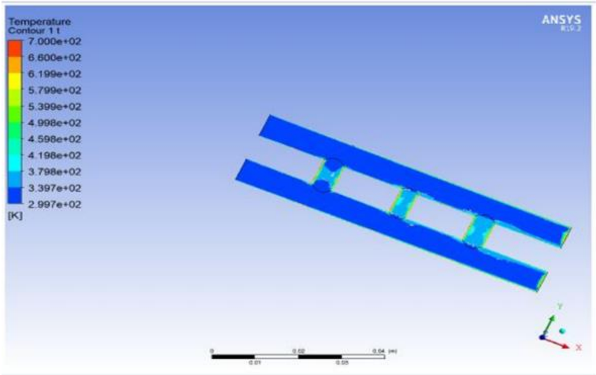

Figure 19. Net cooling channel temperature contours

Figure 20 show cases contour plots of fluid velocity, offering a detailed visual analysis of the fluid dynamics within the system's bends. Strikingly, the data indicates a surge in fluid velocity specifically around the corner regions, reaching a zenith at an extraordinary 179 m/s. These observations not only highlight the intricacies of fluid flow within constrained geometries but also underline the need for meticulous design considerations, especially when dealing with high-velocity flow conditions.

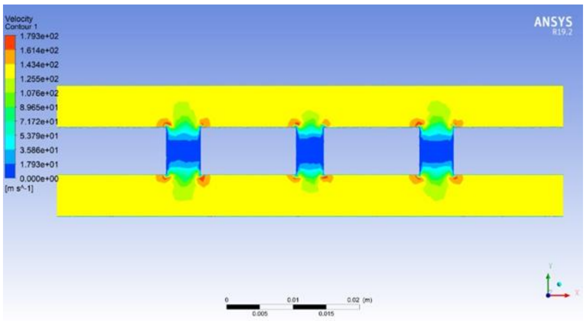

Figure 20. Net cooling channel velocity contours

Figure 21 presents the introduced pressure contour plots that offer valuable insights into the system's dynamics. These contours reveal an interesting observation: pressure levels begin to elevate notably at the Net channels, which have been designed with an angle of 90 degrees. The maximum pressure recorded within the system reaches an impressive 6874 Pascals (Pa). Furthermore, as the channels progress towards their termination, the author discovered a substantial pressure drop, with the pressure eventually decreasing to 1736 Pa. This information highlights the impact of channel design on pressure distribution throughout the system.

Figure 22 demonstrates the relationship between the friction factor and Reynolds number, with a focus on the bends in the cooling channels. Three critical locations within the Net cooling channel were specifically chosen for analysis: locations A, B, and C, these points are of particular interest due to the resistance encountered by the flow, resulting from the variations in the geometric configuration. Consequently, these locations are pivotal in understanding the impact of drag force, especially in relation to the pressure drop.

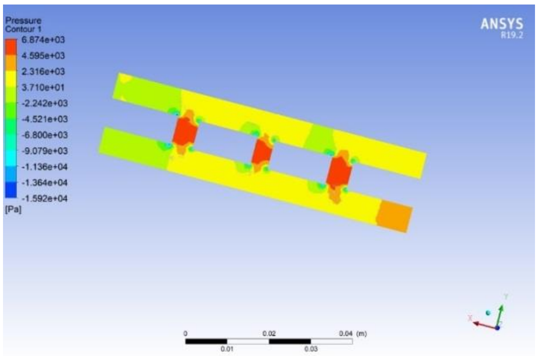

Figure 21. Net cooling channel pressure contours

As depicted in Figure 22, a notable peak in the friction factor, reaching 1.2 at location C, is observed at location when the Reynolds number is 10,000 throughout the channel. However, as the Reynolds number increases to 50,000, there is a marked decrease in the friction factor at all selected locations. This indicates a substantial effect of the Reynolds number on the friction factor, particularly at critical junctures like the turns in the channel. The cooling effect will be highly dependent on the speed variations and a minimum pressure to maintain the flow within the channel is inevitable, as seen in pressure variation contours in Figure 21. The findings call for further investigation into the fluid dynamics at these critical junctures to optimize cooling efficiency.

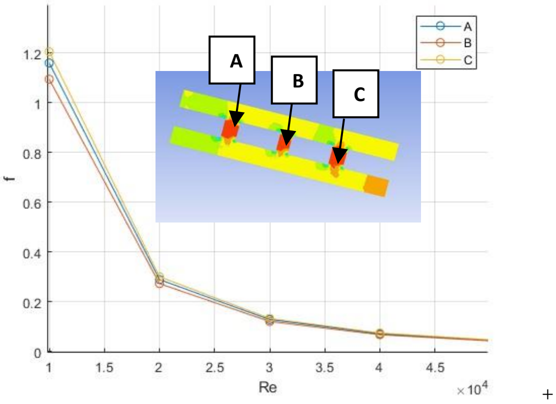

Figure 22. The variation of fraction factor with Reynolds number for Net cooling channels

Figure 23 sheds light on the interplay between drag force and Reynolds number within the context of net cooling channels. Notably, the calculated values reveal that the maximum drag force occurs at location A, which is the initial bend in the cooling channel. On a positive note, the flow pressure is adequate to flow through the channel, carrying sufficient momentum energy to facilitate the cooling process. This is evident in the velocity contours shown in Figure 20. Interestingly, this level of drag force remains consistent across a range of Reynolds numbers, from 10,000 to 50,000. This unchanging behavior of the drag force, across a wide range of Reynolds numbers, indicates a certain robustness that could be significant for understanding fluid flow properties, particularly in systems that operate within these Reynolds number boundaries.

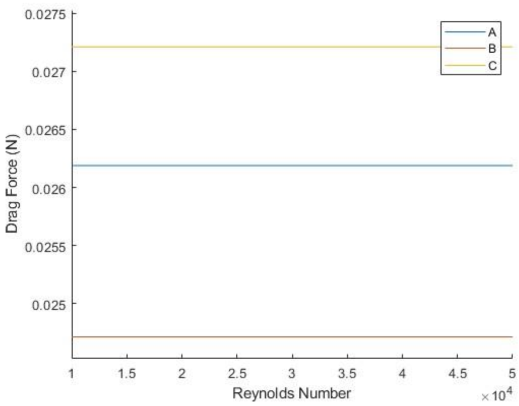

Figure 23. The variation of Drag force with Reynolds number

3.1.3. Investigation performance for jet impingement cooling channels optimization design

Jet impingement type cooling channel, which is a special network of cooling channels, was designed in a web-shape manner at the trailing edge of the blade. This network of channels is close to the jet impingement channel in terms of design proposed by (Glynn, *et al.*, 2005). Figure 24 presents a trend of velocity flow in terms of velocity vectors within the jet impingement type cooling channels. The velocity reaches an elevated level of approximately 115.992 m/s in the main impingement sections and distributes to subsections of the cooling channel. This high-velocity zone could be a critical factor in understanding the unanticipated HTC results.

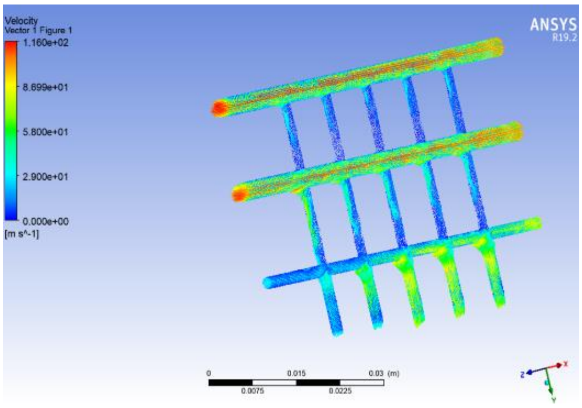

Figure 24. Jet impingement cooling channels velocity vectors' contours

Figure 25 presents the temperature contours within the jet impingement type cooling channel. The temperature within the channels varies from 465.3 K to 658.3 K, demonstrating the heat (temperature) distribution within the blade.

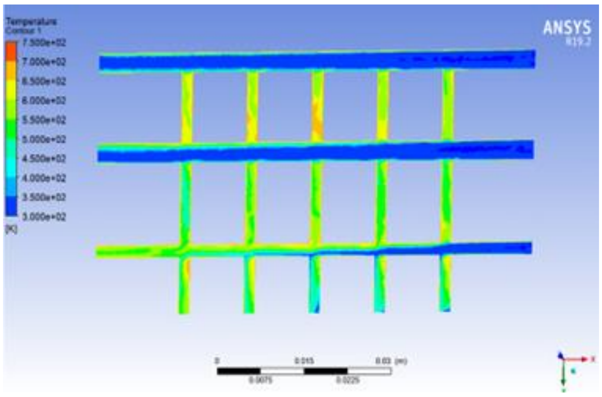

Figure 25. Jet impingement cooling channel temperature contours

Figure 26 elucidates the pressure contour plots, shedding light on the intricacies of the system's dynamics. A striking feature emerges at the Jet impingement cooling channels, specifically designed at a 90-degree angle. At this point, the pressure escalates, peaking at an impressive 4281 Pascals (Pa). As the channels extend towards their endpoints, a marked decline in pressure is observed, plummeting to as low as 1320 Pa. This data underscores the significant role that channel geometry plays in modulating pressure distribution across the channel.

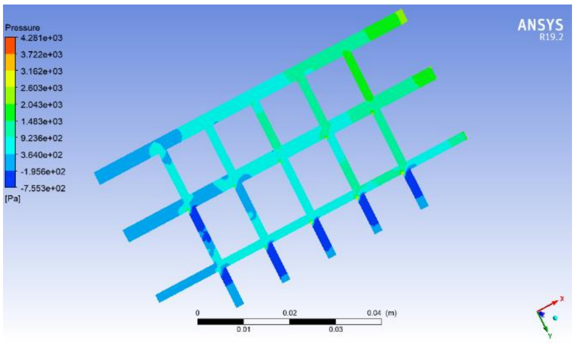

Figure 26. Jet impingement cooling channel pressure contours

Figure 27 illustrates the most important flow relationship between the friction factor and Reynolds number. As the jet impingement type is very complicated in configuration, therefore, for simplicity, 15 locations were chosen, each demonstrating a joint location in the channel. The friction factor was calculated at each location with respect to the Reynolds number. The data indicates an apex in fraction factor, reaching a value of 0.027 at the designated point 7, corresponding to a Reynolds number of 10,000. Conversely, an escalation of the Reynolds number to 50,000 manifests a notable decrement in the friction factor, plummeting to a value of 0.0056. Such variations manifest the sensitivity of the friction factor to fluctuations in Reynolds numbers, particularly at geometrically complex regions, i.e., bends in the cooling channels. These Reynolds number-based variations provide the foundation for the further investigations into thermal management strategies for cooling channel heat transfer.

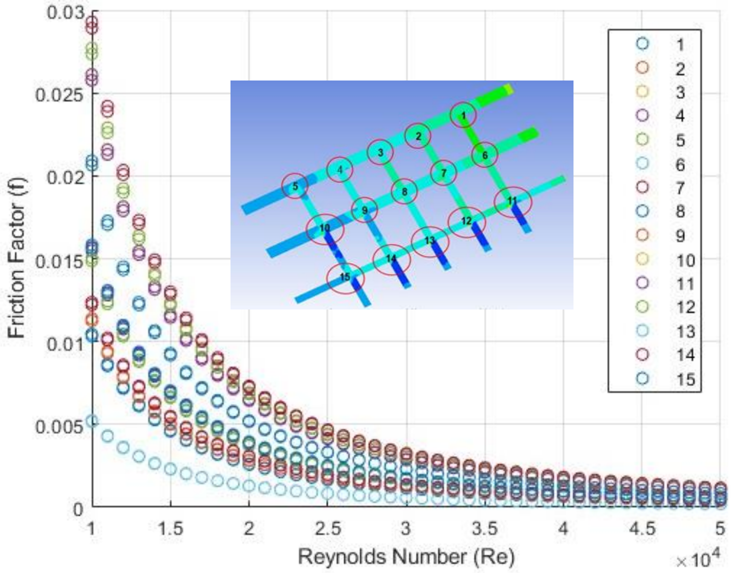

Figure 27. The variation of fraction factor with Reynolds number for jet impingements cooling channels

In Figure 28, a rigorous analysis is presented that delves into the complex interrelations between drag force and Reynolds numbers, specifically in the environment of jet impingement cooling channels. According to the derived data, the highest drag force is located at position 7, registering a value of 0.0007 N, fortunately, the flow pressure is sufficient to navigate the channel, maintaining enough momentum energy to execute the cooling function, as illustrated by the velocity vectors presented in Figure 24. Remarkably, this drag force level decreases across Reynolds numbers ranging from 10,000 to 50,000. Intriguingly, as the Reynolds number advances to 50,000, a systematic decline in the average drag force is observed. This invariant nature of the drag force over an expansive Reynolds number regime signifies a degree of resilience, which could be pivotal for elucidating the fluid dynamic characteristics within systems that operate under such Reynolds number parameters. This observation warrants further exploration to decipher its implications for optimizing fluid flow and cooling efficiency.

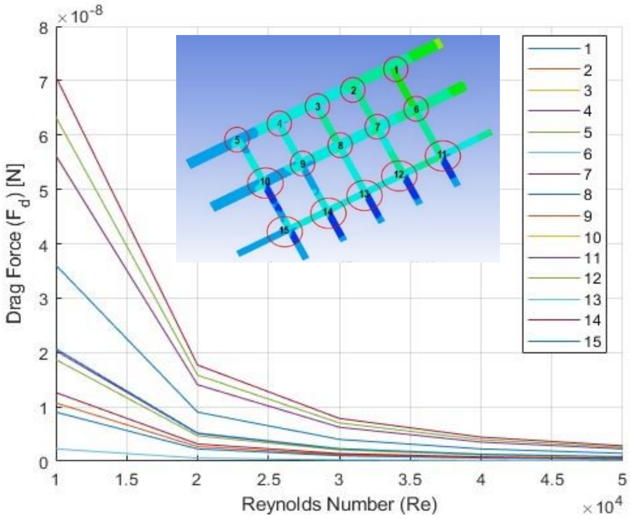

Figure 28. The variation of drag force with Reynolds number

3.1.4. Validation and comparison

This section presents a comparative analysis of the results derived from the three distinct cooling channel designs: U-bend, Net type, and Jet impingement type. A key focus of this analysis is the Nusselt number ratio, a vital parameter in evaluating flow heat transfer efficiency. This ratio, represented as Nua/Nu0, compares the average Nusselt number (N_{ua}) with the reference Nusselt number (N_{u0}) (Yang *et al.*, 2017).

The significance of the Nusselt number ratio in this context is its capability to accurately gauge the efficiency of heat transfer processes. A higher N_{ua}/N_{u0} ratio signifies enhanced convective heat transfer efficiency relative to conductive heat transfer. This efficiency is paramount in practical applications, such as cooling channels, where it is essential for maintaining optimal operational temperatures and ensuring the durability and dependability of the equipment. Furthermore, the observed variations in the Nusselt number ratio across different cases underscore the profound influence of design choices and operational parameters on the efficacy of heat transfer. This insight is instrumental in guiding the optimization of cooling channel designs for improved performance.

The data reveals an initial decline in the Nusselt number ratio (Nu_a/N_{u0}) for all cases, followed by an increase in the Reynolds number (Re). Notably, the Jet Impingement Cooling Channel (Case 3) and the U-Bend Cooling Channel Type (Case 1) demonstrate more significant improvements compared to the Net Cooling Channel (Case 2). The guide vane's thickness emerges as a critical factor influencing thermal exchange at the tip-wall. As illustrated in Figure 29, at a Reynolds number of 60,000, the Jet Impingement Cooling Channel Type (Case 3) exhibits a significant increase of 25.3% in the Nusselt number ratio (Nu_a/N_{ua}). This enhancement is primarily due to the increased fluid acceleration in the outer region of the Jet channels. Specifically, the significant increase in the (Nu_a/N_{u0}) ratio for the Jet Impingement Cooling Channel underlines the effectiveness of this design in enhancing heat transfer, especially at higher Reynolds numbers.

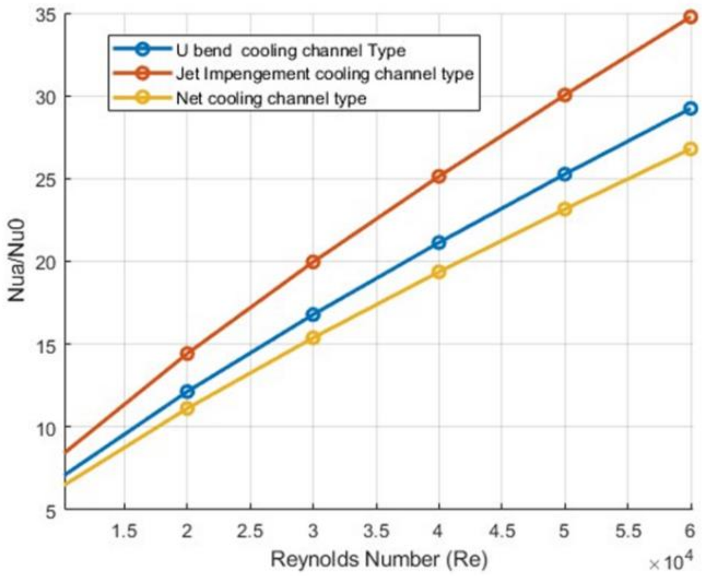

Figure 29. The variation ratio N_{ua}/N_{u0} with Reynolds number for different cooling channels

The assessment of a channel's overall performance heavily relies on its frictional characteristics. Figure 30 illustrates the variations of f/f_o with Reynolds number (Re) for all considered cases. The data from the graph highlights, when Reynolds Number (Re) reaches 20,000, Net cooling channels (Case 2) stand out with a remarkable 25.7% reduction in drag. However, it's essential to note that excessively thick turning vanes can increase channel friction accordingly. This phenomenon occurs because as the thickness of the guide vanes increases, the flow area at the channel's corners decreases, leading to increased resistance due to the reduced cross-sectional area of the basin. While at Re equal 30,000, Jet impingement type cooling channel (Case 3) has reduction in drag with 10.56 % compared to the Net cooling channels (Case 2), and up to 20 % reduction than U-bend cooling channels (Case 1).

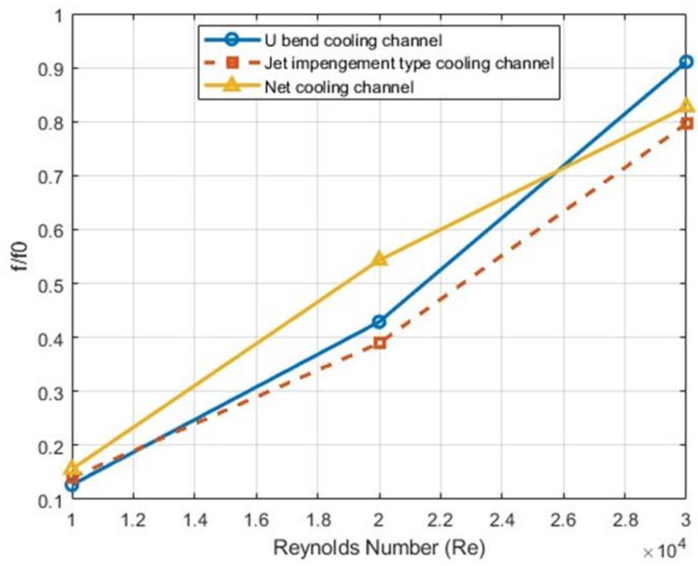

Figure 30. The variation f/f_0 with Reynolds number for different cooling channels

The enhancement in the channel's thermal transfer efficiency often comes at the cost of diminished frictional performance. The Thermal Performance (TP) metric offers a more holistic view by simultaneously accounting for both heat exchange and friction characteristics, thereby providing a well-rounded assessment of the channel's overall performance. Figure 31 illustrates how Thermal Performance (TP) varies with Reynolds Number (Re) across different channels. Initially, as Re escalates, the TP for each channel experiences a decline, reaching its lowest point around Re = 25,000. This phenomenon is largely attributed to minimal advancement in heat exchange levels and a noticeable uptick in channel friction at lower Re values. Subsequently, as Re continues to rise, heat transfer efficiency notably improves, leading to a corresponding increase in TP. Within the lower Re range (10,000 to 30,000), when the Reynolds Number (Re) is at 10,000, the TP in Net cooling channel (case 2) sees an improvement of 3.5%. However, an overly thick internal channels net can result in significant friction losses. In the Re range of 20,000 to 30,000, Net cooling channel (case2) doesn't perform as well in terms of TP as (Case 1) does. Jet impingement type (Case 3) showed better thermal performance at Re 20,000 with 11.27 % than U-bend cooling channel (Case 1). This leads to a gradual outperformance of jet impingement (case 3) in TP compared to other channel configurations. Based on these observations, it can be projected that Jet impingement type cooling channels (Case 3) will offer the most balanced thermal performance when Re exceeds.

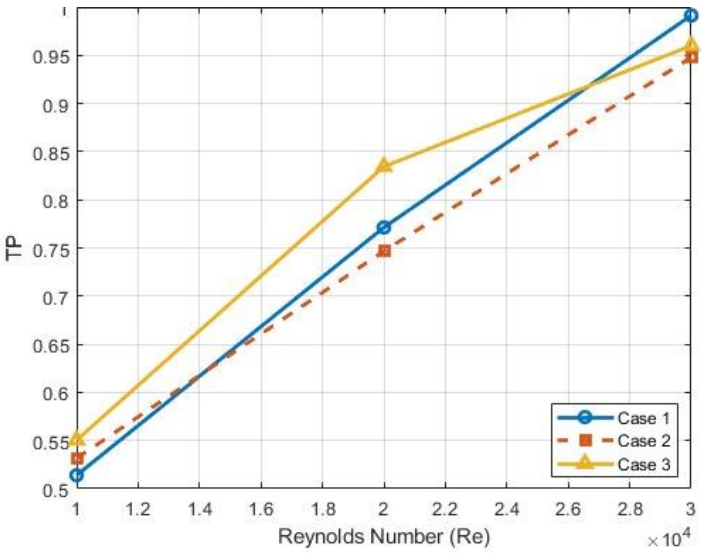

Figure 31. The variation TP with Reynolds number for different cooling channels

4. Discussion

The comprehensive analysis conducted in this study reveals that the unique jet impingement-type cooling channels consistently outperform other types evaluated. These channels, characterized by their jet impingement mechanisms, exhibit superior heat transfer capabilities.

However, given the complexity and variability observed in the performance of these systems, there is a clear indication of the necessity for more sophisticated predictive models for cooling channel design.

While this study lays a robust groundwork, it also highlights the imperative for further research, particularly in the realm of precision-tuning design parameters tailored to specific application needs. The ultimate objective extends beyond mere comprehension of the influencing factors; it encompasses the mastery and manipulation of these elements to realize a fully optimized cooling channel system.

5. Conclusions

In this investigation, thoroughly examine the cooling attributes of various channel configurations. Based on the findings are:

1. The data reveals an initial decline in the Nusselt number ratio (N_{ua}/N_{uo}) for all cases, followed by an increase in the Reynolds number (Re). Notably, the Jet Impingement Cooling Channel (Case 3) and the U-Bend Cooling Channel Type (Case 1) demonstrate more significant improvements compared to the Net Cooling Channel (Case 2). The guide vane's thickness emerges as a critical factor influencing thermal exchange at the tip-wall.
2. At Reynolds number of 60,000, the Jet Impingement Cooling Channel Type (Case 3) exhibits a significant increase of 25.3% in the Nusselt number ratio (N_{ua}/N_{uo}). This enhancement is primarily due to the increased fluid acceleration in the outer region of the Jet channels. Specifically, the significant increase in the (N_{ua}/N_{uo}) ratio for the Jet Impingement Cooling Channel underlines the effectiveness of this design in enhancing heat transfer, especially at higher Reynolds numbers.
3. The data from the graph highlights, when Reynolds Number (Re) reaches 20,000, Net cooling channels (Case 2) stand out with a remarkable 25.7% reduction in drag. However, it's essential to note that excessively thick turning vanes can increase channel friction accordingly. This phenomenon occurs because as the thickness of the guide vanes increases, the flow area at the channel's corners decreases, leading to increased resistance due to the reduced cross-sectional area of the basin. While at Re equal 30,000, Jet impingement type cooling channel (Case 3) has reduction in drag with 10.56 % compared to the Net cooling channels (Case 2), and up to 20% reduction than U-bend cooling channels (Case 1).
4. The drag force for U-channels remained constant at 0.25 N across an extensive Re range (10,000 to 50,000). For Net channels, the drag force stabilized at 0.0272 N, while the Jet impingement cooling channel registered a drag force of 0.0007 N. Interestingly, a progressive decline in average drag force was observed as Re increased to 50,000. This uniform behavior indicates a form of robustness, which may be critical for understanding fluid dynamics in such operational conditions.
5. The Thermal Performance (TP) metric offers a more holistic view by simultaneously accounting for both heat exchange and friction characteristics, thereby providing a well-rounded assessment of the channel's overall performance. Within the lower Re range (10,000 to 30,000), when the Reynolds Number (Re) is at 10,000, the TP in Net cooling channel (Case 2) sees an improvement of 3.5%. However, an overly thick internal channels net can result in significant friction losses. In the Re range of 20,000 to 30,000, Net cooling channel (case2) doesn't perform as well in terms of TP as (case1) does. Jet impingement type (Case 3) showed better thermal performance at Re 20,000 with 11.27 % than U-bend cooling channel (Case 1).

The study examined the thermal and hydraulic characteristics of various cooling channel configurations at different Reynolds numbers (Re). Key findings indicate that slimmer turning vanes are more effective in reducing drag and improving thermal performance Net cooling channel (Case 2) showed promising results in the (N_{ua}/N_{uo}) ratio at Re range of 10,000 to 50,000, while Jet impingement type (Case 3) excelled in drag reduction at Re=30,000. Intriguingly, drag force remained constant across extensive Re ranges, suggesting a form of robustness in fluid dynamics. The results have significant implications for optimizing cooling efficiency in different operational conditions.

References

1. Ackert, S. (2011) *Engine maintenance concepts for financiers elements of turbofan shop maintenance costs.* Available at: http://www.aircraftmonitor.com/uploads/1/5/9/9/15993320/ engine_mx_concepts_for_financiers___v2.pdf (Accessed: September 1, 2011).
2. Afanasyev, V.N., Chudnovsky, Ya.P., Leontiev, A.I., Roganov P.S. (1993) Turbulent flow friction and heat transfer characteristics for spherical cavities on a flat plate. *Experimental Thermal and Fluid Science*, 7(1), 1–8. Available at: https://doi.org/10.1016/0894-1777(93)90075-T.
3. Al-Obaidi, A. R., Chaer, I. (2021) Study of the flow characteristics, pressure drop and augmentation of heat performance in a horizontal pipe with and without twisted tape inserts. *Case Studies in Thermal Engineering*, 25. https://doi.org/10.1016/j.csite.2021.100964.
4. ANSYS Manual. (2006) Fluent 6.2 Documentation File.
5. Brown, G.O. (2002) The History of the Darcy-Weisbach Equation for Pipe Flow Resistance. In: *Environmental and Water Resources History Proceedings*. Reston, VA: *American Society of Civil Engineers*, 34–43. Available at: https://doi.org/10.1061/40650(2003)4.
6. Chyu, M. (1997) Concavity enhanced heat transfer in an internal cooling passage. In: *Proceedings of the ASME 1997 International Gas Turbine and Aeroengine Congress and Exhibition.* https://www.academia.edu/77268876/Concavity_Enhanced_Heat_Transfer_in_an_Internal_Cooling_ Passage (Accessed: 1 June 1997).
7. Coletti, F., Scialanga, M., Arts, T. (2012) Experimental investigation of conjugate heat transfer in a rib-roughened trailing edge channel with crossing jets, *Journal of Turbomachinery*, 134(4). https://doi.org/10.1115/1.4003727.
8. Elmenshawy, A.A.A.E., Alomar, I. (2022) Statistics and Investigation of CF6 Jet Engines Hot Section Failures. In: *Reliability and Statistics in Transportation and Communication. RelStat 2021*. Lecture Notes in Networks and Systems, 410, 88–98. Springer, Cham 2022. https://doi.org/10.1007/978-3-030-96196-1_9.
9. Glynn, C., O’Donovan, T. and Murray, D. (2005) Jet impingement cooling. In: *Proceedings of the 9th UK National Heat Transfer Conference*, 5–6. Manchester, UK.
10. Hylton, L. D., York, R.E. (1983) Analytical and experimental evaluation of the heat transfer distribution over the surfaces of turbine vanes. *NASA Contractor Report*. Available at: https://ntrs.nasa.gov/citations/19830020105.
11. Moon, H.K., O’Connell, T., Glezer, B. (2000) Channel height effect on heat transfer and friction in a dimpled passage. *Journal of Engineering for Gas Turbines and Power,* 122(2), 307–313. https://doi.org/10.1115/1.483208.
12. Nikora, V. (2006) Hydrodynamics of aquatic ecosystems. *Acta Geophysica*, 55(1), 3–10. DOI:10.2478/s11600-006-0043-6.
13. Nirmalan, V., Hylton, L.D. (1989) An experimental study of turbine vane heat transfer with leading edge and downstream film cooling. *Heat Transfer; Electric Power; Industrial and Cogeneration. American Society of Mechanical Engineers*, 4. https://doi.org/10.1115/89-GT-69.
14. Nozhnitsky, Y.A. (2018) The problem of ensuring reliability of gas turbine engines. In: *IOP Conference Series: Materials Science and Engineering*, 302, 012082. https://doi.org/10.1088/1757-899X/302/1/012082.
15. Organ, A.J. (2007) Counter-flow spiral heat exchanger – Spirex, in the air engine. Elsevier, 29–38. https://doi.org/10.1533/9781845693602.1.29.
16. Rossman, C.D. (2016) *Analysis of a coupled micro-and triple-impingement cooling analysis of a coupled micro-and triple-impingement cooling configuration in the C3X vane configuration in the C3X vane*. https://commons.erau.edu/edt.
17. Shen, Zh., Qu, H.,Zhang, D., Xie, Y. (2013) Effect of bleed hole on flow and heat transfer performance of U-shaped channel with dimple structure. *International Journal of Heat and Mass Transfer*, 66, 10–22. https://doi.org/10.1016/j.ijheatmasstransfer.2013.07.008.
18. Uysal, U., Li, P.-W., Chyu, M.K., Cunha, F.J. (2006) Heat transfer on internal surfaces of a duct subjected to impingement of a jet array with varying jet hole-size and spacing. *Journal of Turbomachinery*, 128(1), 158–165. https://doi.org/10.1115/1.2101859.
19. Wang, J., Sunden, B., Zeng, M., Wang, Q. (2015) Film cooling effects on the tip flow characteristics of a gas turbine blade. *Propulsion and Power Research*, 4(1), 9–22. https://doi.org/10.1016/j.jppr.2015.02.003.
20. Wang, K., Li, H. Zhu, J. (2014) Experimental study of heat transfer characteristic on jet impingement cooling with film extraction flow. *Applied Thermal Engineering*, 70(1), 620–629. https://doi.org/10.1016/j.applthermaleng.2014.05.077.

21. Wang, L., Wang, S., Wen, F., Zhou, X., Wang, Zh. (2018) Heat transfer and flow characteristics of U-shaped cooling channels with novel wavy ribs under stationary and rotating conditions. *International Journal of Heat and Mass Transfer*, 126, 312–333. https://doi.org/10.1016/j.ijheatmasstransfer.2018.05.123.
22. Xu, T., Shi, D., Zhang, D., Xie, Y. (2023) Flow and heat transfer characteristics of the turbine blade variable cross-section internal cooling channel with turning vane. *Applied Sciences*, 13(3), 1446. https://doi.org/10.3390/app13031446.
23. Yamane, Y., Ichikawa, Y., Yamamoto, M. Honami, Sh. (2012) Effect of injection parameters on jet array impingement heat transfer. *International Journal of Gas Turbine, Propulsion and Power Systems*, 4(1), 27–34. https://doi.org/10.38036/jgpp.4.1_27.
24. Yang, Sh.-F., Wu, H.-W., Han, J.-Ch., Zhang, L., Moon, H.-K. (2017) Heat transfer in a smooth rotating multi-passage channel with hub turning vane and trailing-edge slot ejection. *International Journal of Heat and Mass Transfer*, 109, 1–15. https://doi.org/10.1016/j.ijheatmasstransfer.2017.01.059.
25. Zaretsky, E. V., Litt, J.S., Hendricks, R.C. (2012) *Determination of turbine blade life from engine field data*. https://ntrs.nasa.gov/search.jsp?R=20120007098.